Acta Cryst. (1997). A53, 576-589

Multislice Method for Large Beam Tilt with Application to HOLZ Effects in Triclinic and Monoclinic Crystals

JIANG HUA CHEN, DIRK VAN DYCK* AND MARC OP DE BEECK†

[a]*EMAT, University of Antwerp (RUCA), Groenenborgerlaan 171, B-2020 Antwerp, Belgium*

(Received 2 October 1996; accepted 10 April 1997)

Abstract

Three existing multislice formulations (MS) that are claimed to be applicable for large beam tilt are introduced in a unified form and the validity of these formulations for large beam tilt is evaluated. It is shown that one formula, which is called MSSBT (the MS for small beam tilt), is valid only for tilt angles less than 6°, but the second one, which is called MSLBT (the MS for large beam tilt), can be used for tilt angles as large as 20°, while the third one yields results very close to the MSLBT results for tilt angles up to 12°. Simulations also show that the accuracy of the MSLBT is independent of the scattering power of the atoms. The reasons for the inaccuracy of these multislice formulations for beam tilt (MSBT) and the differences between the three MSBT formulations are discussed based on the complete Schrödinger equation, which includes back-scattering effects. For calculating the higher-order Laue-zone (HOLZ) effects from triclinic and monoclinic crystals, it is pointed out that the slices have to be cut parallel to the *ab* plane of the crystal and MSBT formulations should be used. The computational formulations for potentials of the crystal slices and the propagator are derived based on the transformations between the crystallographic coordinate system and the working coordinate system. Calculations of the HOLZ reflections for the monoclinic crystal $Na_2Ti_3O_7$ [001] are carried out. It is shown that for triclinic and monoclinic (when the beam direction is along the *c* axis) crystals HOLZ effects dynamically influence not only the intensity but also the symmetry of zero-order Laue-zone (ZOLZ) diffraction patterns. Hence, in that case, the projection approximation for simulating the HRTEM images may not be used.

1. Introduction

For quantitative electron microscopy, accurate dynamical calculations of multiple electron scattering in the specimen are essential since the analysis of experimental data depends entirely on theoretical simulations. Up to now, there have been many dynamical theories or methods for calculating high-energy electron diffraction (HEED) and imaging and each of them has its own advantages for a particular purpose (Wang, 1995). The multislice theory or method (MS), originally proposed by Cowley & Moodie (1957), is particularly suitable for the dynamical calculation when a large number of reflection beams has to be included. The MS can include not only zero-order Laue-zone (ZOLZ) but also higher-order Laue-zone (HOLZ) reflections as well, accurately up to the modified Schrödinger equation for HEED (Goodman & Moodie, 1974; Chen, Op de Beeck & Van Dyck, 1996). Because of its computational capability, the MS is believed to be the most efficient procedure for many cases of HEED and imaging (Spence & Zuo, 1992; Wang, 1995).

However, it is still a problem for the MS to calculate HOLZ effects from triclinic or monoclinic (when the incident electron beam is along the *c* axis) crystals. The difficulty for the MS in such a case is that, when the slices are cut perpendicular to the beam direction, both the size of each slice and the total number of slices needed for the calculation become infinite and therefore calculations of the phase gratings are impossible. The only way to avoid this slicing difficulty, as will be shown, is that the slices have to be taken parallel to the *ab* plane of the crystal lattice but the multislice method for beam tilt (MSBT) should allow for a large beam tilt. However, this immediately gives rise to another important problem: for what magnitudes of tilt angle are the existing MSBT formulations valid or accurate?

Currently, there are several different MSBT formulations (*e.g.* Cowley, 1981; Van Dyck, 1980; Ishizuka, 1982; Wang, 1995). These formulations are identical for normal illumination but different for inclined illuminations. This implies that the validity of MSBT formulations is limited by the tilt angle. Although we know that the MS without beam tilt can be as accurate as the modified Schrödinger equation for HEED, which neglects back-scattering effects, and we also know that if the tilt angle is not too large, perhaps a few degrees, the MSBT should work as well as the MS without tilt (Cowley, 1981), the validity of the MSBT formulations has so far never systematically been tested for different tilt angles. Hence, in order to use the existing MSBT formulations correctly, it is important to test up to what

† Postdoc Researcher of the National Fund for Scientific Research (Belgium).

ISSN 0108-7673

tilt angle they can work with the same accuracy as the MS without tilt.

In the present work, three existing MSBT formulations are first introduced in a unified form. Secondly, using a special monoclinic structure, the validity of the three MSBT formulations is numerically checked for a series of tilt angles by the MS without tilt. Finally, the HOLZ reflections from some monoclinic structures are calculated with one of the tested MSBT formulations.

It should be stressed that only in this particular work is the multislice method divided into the multislice formula without beam tilt (MS) and the multislice formulations for beam tilt (MSBT).

2. Formulations and theoretical schemes

2.1. *Multislice formulations for beam tilt (MSBT)*

In this section, three existing MSBT formulations are introduced in a unified form so as to clearly determine the differences between these formulations. First, we will present two MSBT formulations by following our previous approaches (Van Dyck, 1980; Chen, Van Dyck, Op de Beeck, Broeckx & Van Landuyt, 1995), then in the unified form we rewrite the third formula, which is derived by Wang, who followed Ishizuka's (1982) method based on the so-called first-principles approach (Wang, 1995).

2.1.1. *Two MSBT formulations.* We now consider the transmission of high-energy electrons in a solid under the inclined illumination as shown Fig. 1. The electron wave function $\Psi(\mathbf{r})$ obeys the time-independent Schrödinger equation:

$$-[(h^2/8\pi^2 m)\Delta_r + eU(\mathbf{r})]\Psi(\mathbf{r}) = (h^2k^2/2m)\Psi(\mathbf{r}). \quad (1)$$

The symbols in (1) have their usual meanings (see *e.g.* Spence & Zuo, 1992). By rewriting the wave function

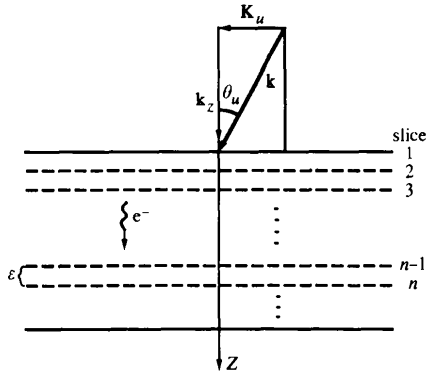

Fig. 1. Illustration of an inclined electron plane wave with wave vector $\mathbf{k}$ incident on a crystal that is assumed to consist of a series of very thin slices, where θ_u is the angle between the incident electron-beam direction and the normal direction of the crystal surface, $\mathbf{k}_z$ and $\mathbf{K}_u$, respectively, are the z component and the xy component of the wave vector $\mathbf{k}$.

(without any loss of generality) as a modulated plane wave with

$$\Psi(\mathbf{r}) = \varphi(\mathbf{r})\exp(2\pi i k_z z), \quad (2)$$

substituting (2) into (1) and neglecting the term $\partial^2\varphi(\mathbf{r})/\partial z^2$, which mainly represents the back-scattering effect (Bird, 1989), we can finally obtain a first-order differential equation for $\varphi(\mathbf{r})$ with

$$\frac{\partial\varphi(\mathbf{r})}{\partial z} = \left[\frac{i}{4\pi k_z}\Delta + \frac{k}{k_z}i\sigma U(\mathbf{r}) + \frac{i\pi\mathbf{K}_u^2}{k_z}\right]\varphi(\mathbf{r}), \quad (3)$$

where σ is the interaction constant, $\mathbf{k}$, $\mathbf{K}_u$ and k_z are defined in Fig. 1 and Δ is the Laplacian operator in the xy plane.

Solving (3) in the multislice scheme, in which the solid film is considered as a series of thin slices with the same slice thickness (Fig. 1) and neglecting some constant factors (Chen, Van Dyck, Op de Beeck, Broeckx & Van Landuyt, 1995), we obtain the first MSBT formula:

$$\begin{aligned}\Phi_n^{\mathbf{K}_u} &= \exp\{\varepsilon_u[(i\lambda\Delta/4\pi) - \lambda\mathbf{K}_u\cdot\nabla \\ &\quad - \pi i\lambda\mathbf{K}_u^2 + i\sigma V_n^p]\}\Phi_{n-1}^{\mathbf{K}_u} \\ &\simeq \exp\{\varepsilon_u[(i\lambda\Delta/4\pi) - \lambda\mathbf{K}_u\cdot\nabla \\ &\quad - \pi i\lambda\mathbf{K}_u^2]\}\exp(i\sigma\varepsilon_u V_n^p)\Phi_{n-1}^{\mathbf{K}_u}, \end{aligned} \quad (4)$$

with the slice potential averaged along $\mathbf{z}$ (the slice plane normal):

$$V_n^p(\mathbf{R}) = (1/\varepsilon)\int_{(n-1)\varepsilon}^{n\varepsilon} U(\mathbf{r})\,dz, \quad (5)$$

where $\Phi_0^{\mathbf{K}_u}(\mathbf{R}) = 1$, ∇ is the gradient operator in the xy plane, $\varepsilon_u = \varepsilon/\cos\theta_u = (k/k_z)\varepsilon$ is the 'slice thickness' measured along the beam direction and $\lambda = 1/k$ is the incident electron wavelength. In (4), the propagator, in reciprocal space (by the Fourier transformation), takes the following form:

$$P(\mathbf{K}, \mathbf{K}_u) = P(\mathbf{K} + \mathbf{K}_u) = \exp[-\pi i\varepsilon_u\lambda(\mathbf{K} + \mathbf{K}_u)^2], \quad (6)$$

where $P(\mathbf{K})$ indicates the normal Fresnel propagator in reciprocal space.

However, the interesting thing is that, instead of (2), if we write the modulated plane wave as $\Psi(\mathbf{r}) = \varphi(\mathbf{r})\exp(2\pi ikz)$ and follow the same derivation procedure as for the first MSBT formula, another MSBT formula can be obtained (Chen, Van Dyck, Op de Beeck, Broeckx & Van Landuyt, 1995):

$$\begin{aligned}\Phi_n^{\mathbf{K}_u} &= \exp\{\varepsilon[(i\lambda\Delta/4\pi) - \lambda\mathbf{K}_u\cdot\nabla \\ &\quad - \pi i\lambda\mathbf{K}_u^2 + i\sigma V_n^p]\}\Phi_{n-1}^{\mathbf{K}_u} \\ &\approx \exp\{\varepsilon[(i\lambda\Delta/4\pi) - \lambda\mathbf{K}_u\cdot\nabla \\ &\quad - \pi i\lambda\mathbf{K}_u^2]\}\exp(i\sigma\varepsilon V_n^p)\Phi_{n-1}^{\mathbf{K}_u}. \end{aligned} \quad (7)$$

The only difference between (4) and (7) is that the slice thickness in (7) is measured along the normal direction

of the slice plane and is independent of the beam tilt, while the 'slice thickness' in (4) depends on the beam tilt. It should be noted that in (4) and (7) the first-order Zassenhaus expansion (Goodman & Moodie, 1974; Van Dyck, 1979) is used to separate the propagator and the phase grating.

2.1.2. *The third formula presented in the unified form.* Ishizuka's original MSBT formula (Ishizuka, 1982) is difficult to rewrite in the form that we used to present the first two formulations. Moreover, the potential in his formula is projected along the incident-beam direction and therefore would be very difficult to calculate when HOLZ effects have to be included. However, following Ishizuka's derivation, Wang (1995) presented a modified formula, for which the potential should be projected along the normal direction of the slice plane. Nevertheless, this formula can be rewritten in the unified form as follows (see Appendix *A*):

$$\Phi_n^{\mathbf{K}_u} = \exp\{\varepsilon[(i\lambda\Delta/4\pi) - \lambda\mathbf{K}_u \cdot \nabla - \pi i\lambda\mathbf{K}_u^2]\} \exp(i\sigma\varepsilon_u V_n^p)\Phi_{n-1}^{\mathbf{K}_u}. \quad (8)$$

We see that in the third formula the propagator is the same as that in (7) but the phase grating is that of (4).

So, following different derivations, different MSBT formulations are obtained. The common feature of all these derivations is the use of the high-energy approximation (*e.g.* Van Dyck & Coene, 1984) or forward-scattering approximation (Ishizuka, 1982), *i.e.* the neglect of back scattering, but the back scattering in each derivation is defined in its own way and this leads to different MSBT formulations. (We will come to this point later in the discussions.) It is also noticed that in Ishizuka's and Wang's derivations the small-angle scattering approximation is stressed to obtain the simplified propagator.

Equations (4), (7) and (8) are the three MSBT formulations that we are going to test numerically with the *FFTMS* algorithm (Ishizuka & Uyeda, 1977). It should be noted that without simulations it is difficult to judge which MSBT formula is more accurate than the others.

2.2. *Theoretical schemes*

In this section, the schemes will be presented to calculate the HOLZ effects from triclinic and monoclinic structures and to test MSBT formulations.

2.2.1. *Scheme for the HOLZ calculation of non-orthogonal crystals.* It is known that the MS (without beam tilt) can calculate HOLZ effects correctly up to the exact solution of the modified Schrödinger equation for HEED if the slice thickness is taken sufficiently thin (Chen, Op de Beeck & Van Dyck, 1996). However, when considering the HOLZ reflection effects from triclinic and monoclinic (if the incident beam is along the *c* axis) structures (Fig. 2*a*), the MS immediately runs into the problem that, since they have to be cut perpendicular to the *c* axis (the incident-beam direction), the slices not only have no periodicity in the *xy* plane, but also cannot repeat themselves in the *z* direction. In reciprocal space (Fig. 2*b*), the situation is that HOLZ spots are not located at the reciprocal-lattice points of the ZOLZ plane but somewhere between these points. So it is impossible to describe the phase gratings for operating the MS calculation.

In order to obtain computable phase gratings, the only way is to make the slices parallel to the *ab* plane, since in this way the obtained slices not only have the periodicity of the *ab* lattice plane but also can repeat themselves by including a shift of $\delta\mathbf{R} = (c/a)\cos\beta\mathbf{a} + (c/b)\cos\alpha\mathbf{b}$ after passing each *ab* lattice plane (Fig. 2*a*), where α and β are the angles of the triclinic lattice defined in Fig. 5(*a*).

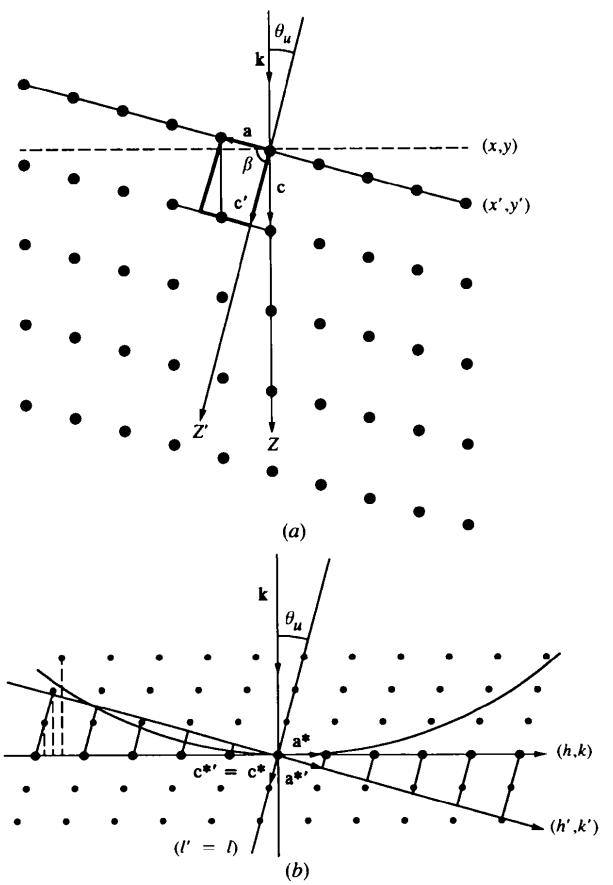

Fig. 2. Illustration of the scheme to calculate the HOLZ effects from a triclinic or monoclinic crystal, showing the slicing difficulty of the MS (without beam tilt) and the feasible way of using the MSBT for the calculation: (*a*) real space; (*b*) reciprocal space with the Ewald sphere, where (h, k) is the ZOLZ plane and (h', k') the working lattice plane.

However, to calculate the diffraction patterns with the phase gratings parallel to the *ab* plane, MSBT formulations should be used, that is, a beam tilt of $|K_u| = (\sin\theta_u/\lambda)$ has to be included in the propagator.

It should be noticed that in making slices parallel to the *ab* plane we in fact create a working lattice plane in reciprocal space (Fig. 2*b*) that is defined by reciprocal-lattice vectors $\mathbf{a}^{*\prime}(= 1/a\sin\gamma)$ and $\mathbf{b}^{*\prime}(= 1/b\sin\gamma)$, so that all the calculated reflection spots are located at lattice points of the working plane. It is also interesting to notice that with respect to the working plane all the original ZOLZ reflections except the central beam become HOLZ reflections. This means that, in order to obtain accurate results with the MSBT, sufficiently thin slices have always to be taken (even when no real HOLZ reflections are involved, see §2.2.2) since for HOLZ effects the multislice approach is only a first-order approximation in slice thickness (Chen, Op de Beeck & Van Dyck, 1996).

2.2.2. *Scheme for testing the MSBT.* In order to use the MSBT to calculate the HOLZ effects for triclinic and monoclinic crystals, first of all, we have to know up to what tilt angle the MSBT formulations are as accurate as the MS and which formula is the best for large beam tilt.

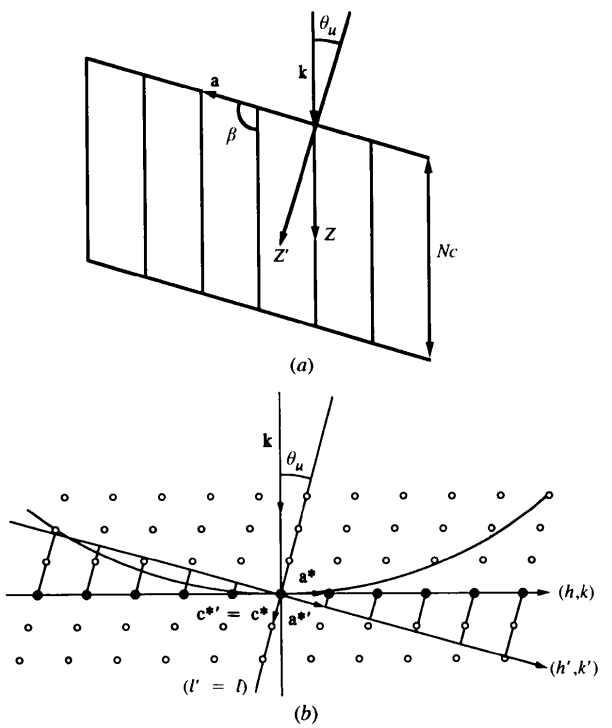

Fig. 3. Illustration of the imaginary monoclinic structure model for testing the MSBT: (*a*) the real space, where the β angle between the *a* axis and the *c* axis is assumed changeable; (*b*) the reciprocal space with the Ewald sphere, where all the higher-order lattice planes (represented by empty circles) are removed.

For this purpose, here we propose an imaginary monoclinic structure (Fig. 3*a*). The structural model can be built up from a real monoclinic crystal by averaging the potential along the *z* direction (the *c* axis), *e.g.* removing all the HOLZ lattice planes (Fig. 3*b*). For such a structure, since there is only a ZOLZ plane, diffraction case (*a*) in Fig. 4 is equivalent to the case in Fig. 4(*b*) - based on the exact solution of the modified Schrödinger equation for HEED - and therefore the case in Fig. 4(*c*) yields the same results as the case in Fig. 4(*d*) where the structure with the projected lattice parameter of $a_0 = a\sin\beta$ is orthogonal so that we can obtain accurate diffraction patterns with the MS procedure. On the other hand, for case (*c*), we can directly carry out the calculation with the MSBT and the obtained results can be compared with those calculated by the MS in case (*d*). Moreover, for such a structure model, the β angle between the *a* axis and the *c* axis can be assumed changeable. In this way, the validity of the MSBT can numerically be checked with the MS for a series of tilt angles.

Again, it should be stressed that, although the potential along the *z* direction is constant, there is potential variation along the *z'* direction. Hence, the original ZOLZ reflections have to be treated as HOLZ effects when we use the MSBT for case (*c*) in Fig. 4, that is, the slices parallel to the *ab* plane have to be cut sufficiently thin.

3. Computational formulations of the MSBT for triclinic crystals

In order to calculate the phase gratings and the propagator of the MSBT from the lattice parameters and structural data of triclinic crystals, the following transformations between the two coordinate systems in Fig. 5 are necessary:

(*a*) In real space,

$$\mathbf{a}' = \mathbf{a}, \quad \mathbf{b}' = \mathbf{b},$$
$$\mathbf{c}' = -[(c/a)\cos\beta]\mathbf{a} - [(c/b)\cos\alpha]\mathbf{b} + \mathbf{c}$$

and

$$x' = x + [(c/a)\cos\beta]z, \quad y' = y + [(c/b)\cos\alpha]z, \quad z' = z. \tag{9}$$

(*b*) In reciprocal space,

$$\mathbf{a}^{*\prime} = \mathbf{a}^* + [(c/a)\cos\beta]\mathbf{c}^*,$$
$$\mathbf{b}^{*\prime} = \mathbf{b}^* + [(c/b)\cos\alpha]\mathbf{c}^*, \quad \mathbf{c}^{*\prime} = \mathbf{c}^*$$

and

$$h' = h, \quad k' = k,$$
$$l' = -[(c/a)\cos\beta]h - [(c/b)\cos\alpha]k + l. \tag{10}$$

3.1. *Calculating the potential of the slices*

Since the crystal potential can be written as

$$V(\mathbf{r}') = V(\mathbf{r}) = \sum_{hkl} U(hkl)\exp[2\pi i(hx + ky + lz)]$$
$$= \sum_{hkl} U(hkl)\exp\big(2\pi i\{hx' + ky' + [1 - h(c/a)\cos\beta - k(c/a)\cos\alpha]z'\}\big), \quad (11)$$

the average potential (along the normal direction of the slice plane) within slice n is

$$V_n^p(\mathbf{R}') = (1/\varepsilon)\int_{(n-1)\varepsilon}^{n\varepsilon} V(\mathbf{r}')\,\mathrm{d}(z'c')$$
$$= \sum_{h,k} U_n'(h,k)\exp[2\pi i(hx' + ky')] \quad (12)$$

with

$$U_n'(h,k) = \sum_l U(hkl)\frac{\sin\{(\pi/m)[l - h(c/a)\cos\beta - k(c/a)\cos\alpha]\}}{\{(\pi/m)[l - h(c/a)\cos\beta - k(c/a)\cos\alpha]\}}$$
$$\times \exp\{2\pi i z_n'[l - h(c/a)\cos\beta - k(c/a)\cos\alpha]\}, \quad (13)$$

where $m = c'/\varepsilon$ and $z_n' = (1/m)(n - \frac{1}{2})$ and the Fourier transform of the potential can be calculated by

$$U(hkl) = (C/\Omega_{\text{cell}})\sum_j f_j(hkl)\exp(-B_j/4d_{hkl}^2)$$
$$\times \exp[-2\pi i(hx_j + ky_j + lz_j)] \quad (14)$$

with C and Ω_{cell}, respectively, a constant and the volume of the unit cell (Self, O'Keefe, Buseck & Spargo, 1983). In (14), (x_j, y_j, z_j) are the coordinates of atom j in the original triclinic unit cell and B_j and f_j, respectively, the Debye–Waller factor (DW) and the atomic scattering factor of atom j. d_{hkl} is the interplanar spacing of reflection planes (hkl).

If only $l = 0$ is included in the potential calculations, the potential variation along the c axis is neglected. This is just the case for the monoclinic structural model that is used to test the MSBT.

3.2. *Propagator for beam tilt*

In the MSBT calculation for triclinic crystals, the propagator in (6) has to be calculated with respect to the working plane in reciprocal space, that is

$$\mathbf{K} = h'\mathbf{a}^{*\prime} + k'\mathbf{b}^{*\prime}$$
$$\mathbf{K}_u = [(a/\lambda)\cos\beta\sin^2\gamma]\mathbf{a}^{*\prime} + [(b/\lambda)\cos\alpha\sin^2\gamma]\mathbf{b}^{*\prime}. \quad (15)$$

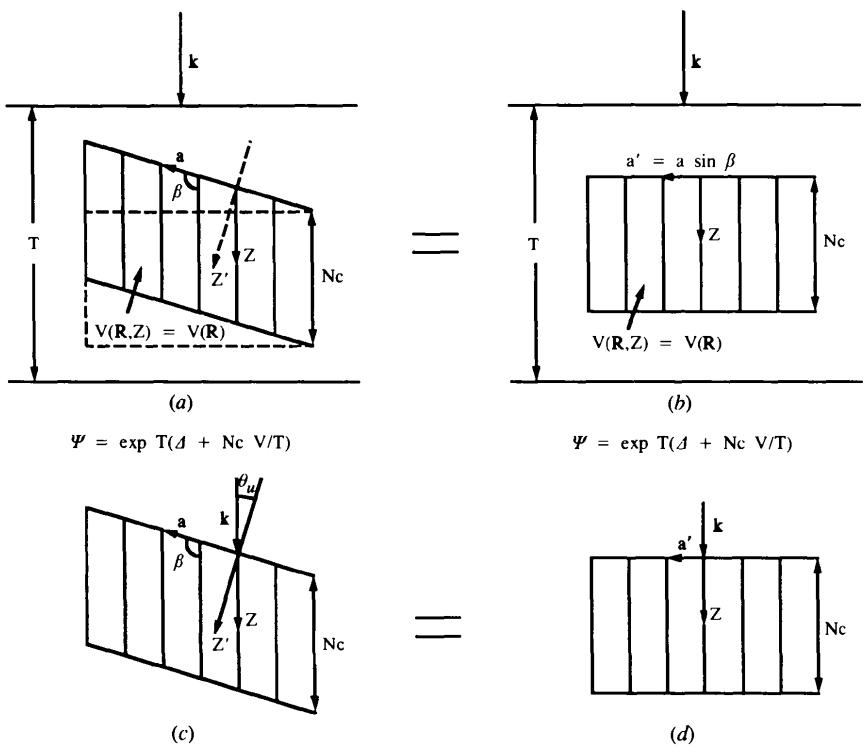

Fig. 4. Demonstration of the equivalencies between diffraction cases (*a*) and (*b*) and (*c*) and (*d*), in which $\Psi_n(\mathbf{R}, T) = \exp\{T[\Delta + NcV(\mathbf{R})/T]\}$ is the exact solution of equation (3), the modified Schrödinger equation for HEED, with short-hand notations: Δ and $V(\mathbf{R})$, the 2D Laplacian operator and the potential multiplied by, respectively, $i\lambda/4\pi$ and $i\sigma$.

Table 1. *Structure data and Debye-Waller factors for the $Na_2Ti_3O_7$ monoclinic crystal, which are used for calculations (Andersson & Wadsley, 1961); the DW factors are assumed values*

Type of atom	Na	Ti	O
Number of atoms	2 × 2	2 × 3	2 × 7
Atom positions:	0.318, 0.75, 0.405	0.9722, 0.75, 0.7194	0.779, 0.75, 0.805
(x_j, y_j, z_j)	0.492, 0.75, 0.846	0.7533, 0.75, 0.3270	0.860, 0.75, 0.527
and	and	0.858, 0.75, 0.0189	0.562, 0.75 0.355
$(1-x_j, 1-y_j, 1-z_j)$	$(1-x_j, 1-y_j, 1-z_j)$	and	0.686, 0.75, 0.115
$a = 0.8571$ nm		$(1-x_j, 1-y_j, 1-z_j)$	0.006, 0.75, 0.255
$b = 0.3804$ nm			0.209, 0.75 0.687
$c = 0.9135$ nm			0.095, 0.75, 0.969
$\beta = 101.95°$			and
			$(1-x_j, 1-y_j, 1-z_j)$
DW factors	0.25	0.20	0.50

4. Calculations

In the present work, a program *FFTMS* written by J. H. Chen is used and calculations are carried out for the [001] zone-axis diffraction of the monoclinic crystal $Na_2Ti_3O_7$ (Andersson & Wadsley, 1961).

First, the accuracies of the MSBT for different tilt angles, from 3 to 30°, are checked by changing the β angle of the monoclinic crystal $Na_2Ti_3O_7$, from 93 to 120°. Moreover, to see whether or not the accuracy of the MSBT is related to the scattering power of the atoms, MSBT calculations are also made for a hypothetical crystal, $Cs_2Ti_3O_7$, which is obtained by simply replacing the lighter atom Na by a heavy atom Cs in the $Na_2Ti_3O_7$ monoclinic structure. Secondly, the differences between the three MSBT formulations are numerically demonstrated by calculations. Finally, calculations of HOLZ effects are carried out for two $Na_2Ti_3O_7$ monoclinic structures: one with the real β angle of 101.95° and another with an assumed β angle of 96°.

The structural data for the monoclinic crystal $Na_2Ti_3O_7$ are listed in Table 1. The Debye-Waller (DW) factors in Table 1 are assumed values since they are not available in the literature. It is noted that the use of the DW factors is very important for damping down the outer large-angle reflections, especially when the HOLZ effects are taken into account (Chen *et al.*, 1996). The accelerating voltage of 200 kV and 128 × 64 sampling points (corresponding to the sampling intervals of 0.067 × 0.059 Å, which are quite sufficient when the DW factors are included) in the *ab* plane are kept fixed for all calculations.

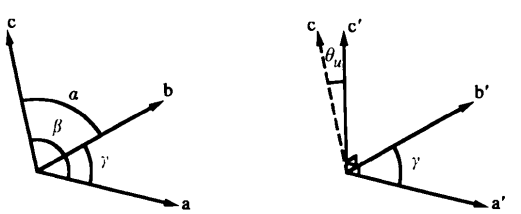

Fig. 5. Illustration of the crystallographic coordinate system for describing triclinic structures and the working coordinate system for performing the MSBT calculation.

5. Calculation results

The results from the numerical tests of the three MSBT formulations are given in Fig. 6 through Fig. 15 and those from the HOLZ calculations of monoclinic structures are demonstrated in Fig. 13 through Fig. 15. The amplitude diffraction patterns (Fig. 13) are printed in such a way that a zero amplitude is set for all the reflections whose amplitudes are less than 3.0×10^{-3} and a fixed maximum value of 7.0×10^{-2} is set for those amplitudes that are larger than this maximum value. In the presented results, the symbols MSLBT, MSSBT and MSMBT, respectively, refer to (4), (7) and (8) (see definitions of these symbols in the *Discussion*).

Figs. 6 and 7 show that the inaccuracy of the MSLBT increases slowly with increasing tilt angle. The MSLBT results are still acceptable for a tilt angle up to 18°, but for tilt angles as large as 30° the errors of the MSLBT are severe. On the other hand, Fig. 8 shows that the accuracy of the MSLBT is independent of the scattering power of the atoms in the crystal, since the deviations of the MSLBT results from the standard MS results are not significantly changed by replacing Na by Cs in the $Na_2Ti_3O_7$ structure. Fig. 9, however, shows that the amplitudes calculated by the MSLBT dramatically change with decreasing slice thickness until a sufficiently small slice thickness is employed.

Comparisons of the results calculated by the three different MSBT formulations are given in Figs. 10, 11 and 12. It is shown that for large tilt angles the MSLBT is much more accurate while for tilt angles less than 3° the three formulations show no differences. In addition, Figs. 10 and 11 show that MSSBT is still good enough for the tilt angle of 6°, while Fig. 12 shows that the MSMBT results are very close to the MSLBT results up to tilt angles as large as 12°.

Finally, the HOLZ reflections calculated by the MSLBT for the $Na_2Ti_3O_7$ monoclinic structure with

the hypothetical β angle of 96° and that with the real β angle of 101.95° are shown in Figs. 13 to 15. It should be noted that the calculated HOLZ diffraction patterns (Fig. 13) are presented in the working plane, not in the normal ZOLZ plane. It is shown in Fig. 15 that the intensity of ZOLZ reflection $h00$ differs from that of $\bar{h}00$. This is an interesting result since it cannot be expected from the projection approximation.

6. Discussion

6.1. *MSBT formulations*

There are several existing MSBT formulations. Some of them are identical (*e.g.* Cowley, 1981; Chen, Wang, Luo, Ding & Cheng, 1995), some are really different. However, the differences between existing MSBT formulations are not always easy to

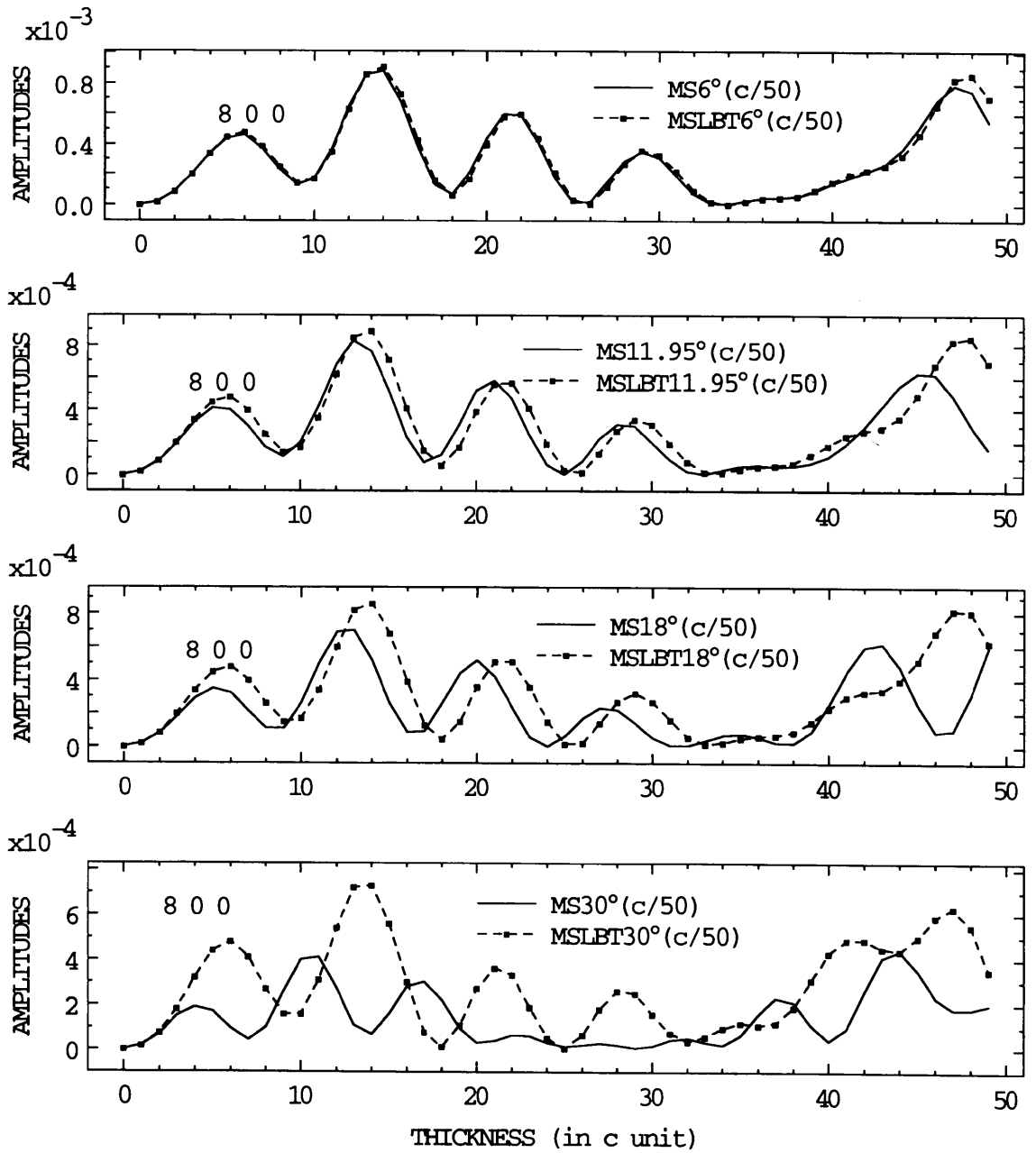

Fig. 6. Plots of the amplitudes of the 800 diffraction beam against crystal thickness, showing the accuracies of the MSBT for different tilt angles, where the symbol MSLBT $x°(c/50)$ represents the result calculated by the MSLBT, equation (4), for the monoclinic structure with an $x°$ angle between the normal direction of the *ab* plane and the *c* axis and the slice thickness is $c/50$, while the symbol MS$x°(c/50)$ indicates the standard result calculated by the multislice method (without beam tilt) for the same structure and the slice thickness used is $c/50$.

see because different authors use different approaches to the multislice theory. In this work, three existing formulations are introduced in a unified form so that the differences between them are summarized as differences in measuring the slice thickness, although, without simulations, it is still difficult to judge which formula is most accurate. It is clear, however, that the accuracy of each MSBT formulation is a function of the tilt angle and the smaller the tilt angle is the more accurate the MSBT formulation will be. When the tilt angle approaches zero, all the formulations converge to the MS formula (with zero tilt), which has been proven to yield the exact solution of the modified Schrödinger equation for HEED when the slice thickness is very small (*e.g.* Goodman & Moodie, 1974). Thus, the MS is the most accurate multislice formula and can therefore serve as the standard for checking the validity of MSBT formulations. In order to do so, however, a special structure has to be used so that the same diffraction patterns can be calculated by both the MS and the MSBT formulations.

We have seen from the calculation results that (4), the formula in which the slice thickness is measured along the incident-beam direction, is good enough at tilt angles up to 20° and (7), the formula in which the slice thickness is measured along the normal direction of the slice plane, is valid for tilt angles less than 6°, while (8), the formula in which the slice thickness for the propagator is taken different from that for the phase grating, yields results very close to those of (4) up to 12°. For small tilt angles (less than 3°), these three formulations yield exactly the same results. For convenience, (4), (7) and (8), respectively, will be called MSLBT (the MS for large beam tilt), MSSBT (the MS for small beam tilt) and MSMBT (the MS for medium beam tilt).

So we see that, for normal simulations of HRTEM image and CBED patterns around a zone axis, the MSSBT is accurate enough since 6 or even 3° covers most experimentally used tilt angles. On the other hand, for a crystal it is always possible to define a new unit cell $(\mathbf{a}', \mathbf{b}', \mathbf{c}')$ so that the incident-beam direction is close to the new $a'b'$ normal. So in many cases it is not necessary to use the MSLBT. But if the surface effects are important, such as for bulk-forbidden surface-allowed diffraction (Marks, 1992), reflection high-energy electron diffraction (RHEED) where the illumination probe itself can be tilted away from the zone axis by more than 6° (see *e.g.* Wang, 1995) and non-orthogonal crystal diffraction, the MSLBT and the MSMBT may be useful.

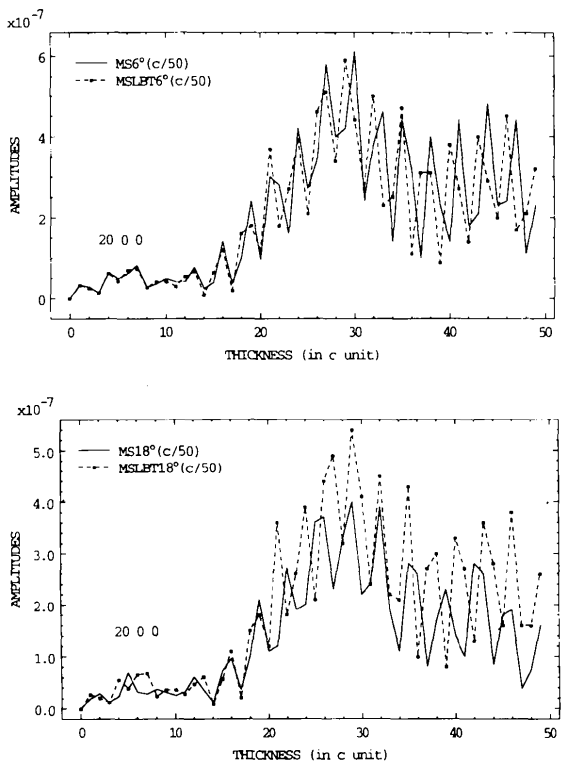

Fig. 7. The same as for Fig. 6 but for the 20,0,0 diffraction beam.

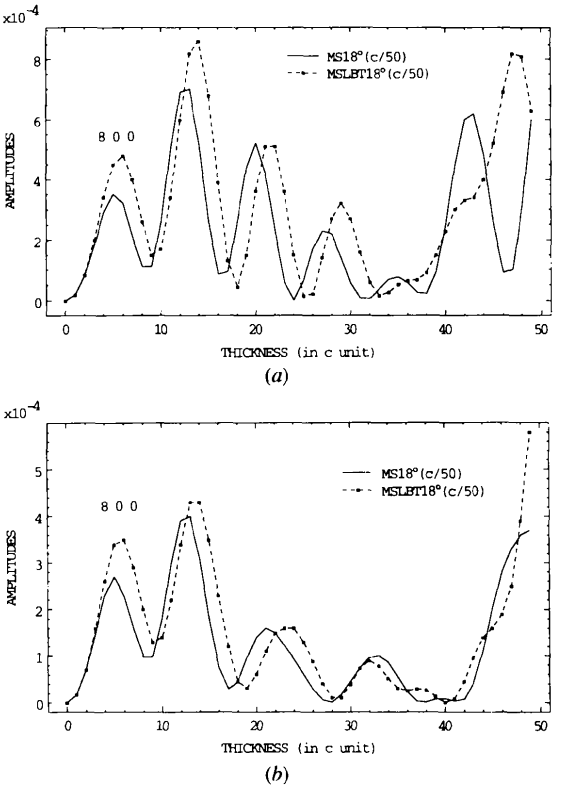

Fig. 8. Plots of the amplitudes of the 800 diffraction beam against crystal thickness showing that the accuracy of the MSBT is independent of the scattering power of the atoms. Meanings of the symbols are the same as in Fig. 6. (*a*) $Na_2Ti_3O_7$, (*b*) $Cs_2Ti_3O_7$.

Although the MSLBT can be used for large beam tilt, it should be stressed that in that case, for the potential calculation, one may no longer use the projection approximation that holds when the c parameter is small and the incident beam is exactly along the c axis. Actually, when the beam is tilted away from the c axis, the potential variation along the c axis becomes 'visible' and should be taken into account. Moreover, to include the potential variation properly, the slice thickness has to be cut sufficiently thin (Chen, Op de Beeck & Van Dyck, 1996). Nevertheless, it is interesting to notice that under the projection approximation (along the normal direction of the slice plane), the MSSBT and the MSLBT become identical except the total crystal thickness for the former ($n\varepsilon$) is shorter than that of the latter [$n\varepsilon_u = n(k/k_z)\varepsilon$]: for $V_1^p = \ldots = V_n^p = \bar{V}$, the MSLBT [equation (4)] becomes $\Phi_n^{\mathbf{K}_u} = \exp\{(n\varepsilon_u)\times [(i\lambda\Delta/4\pi) - \lambda\mathbf{K}_u\cdot\nabla - \pi i\lambda\mathbf{K}_u^2 + i\sigma\bar{V}]\}\Phi_0^{\mathbf{K}_u}$, while the MSSBT [equation (7)] will become $\Phi_n^{\mathbf{K}_u} = \exp\{(n\varepsilon)\times [(i\lambda\Delta/4\pi) - \lambda\mathbf{K}_u\cdot\nabla - \pi i\lambda\mathbf{K}_u^2 + i\sigma\bar{V}]\}\Phi_0^{\mathbf{K}_u}$. However, if the potentials in each slice are different, slice operators will not be commutative and these two formulations will differ in an additional way. This is the case shown in Figs. 10 and 11 for which the MSBT calculations are made with different phase gratings so as to describe the potential variation along the z' direction.

Theoretically, it is interesting to know why the MSBT is not as accurate as the MS (without beam tilt). The main reason for this, we believe, is that the normal high-energy approximation that yields both the MS and MSBT may not hold for large beam tilt, Actually, in the case of beam tilt, the back-scattering effects should be represented by $\partial^2\varphi(\mathbf{r})/\partial z_u^2$ instead of $\partial^2\varphi(\mathbf{r})/\partial z^2$ (Fig. 16*a*). Since $\varphi(x, y, z) = \varphi(x_u, y_u, z_u)$, the relation between these two 'back-scattering' terms can easily be found:

$$\frac{\partial^2\varphi}{\partial z^2} = \frac{\partial^2\varphi}{\partial x_u^2}u_x^2 + \frac{\partial^2\varphi}{\partial y_u^2}u_y^2 + \frac{\partial^2\varphi}{\partial z_u^2}u_z^2 + 2\left(\frac{\partial^2\varphi}{\partial x_u\partial y_u}u_xu_y + \frac{\partial^2\varphi}{\partial y_u\partial z_u}u_yu_z + \frac{\partial^2\varphi}{\partial z_u\partial x_u}u_zu_x\right) \tag{16}$$

with

$$u_x = \frac{\partial x_u}{\partial z}, \quad u_y = \frac{\partial y_u}{\partial z}, \quad u_z = \frac{\partial z_u}{\partial z}. \tag{17}$$

So we can see that, neglecting $\partial^2\varphi(\mathbf{r})/\partial z^2$ in the case of beam tilt, we in fact neglect not only a (large) part of the back scattering but also a (small) part of the forward scattering as well.

This situation can clearly be illustrated in a reciprocal-space configuration (Fig. 16*b*): In the case of beam tilt, the back scattering covers all the wave vectors pointing towards the part ACB of the Ewald sphere while the forward scattering covers all those pointing towards the part AEB of the sphere. However, in the normal high-energy approximation,

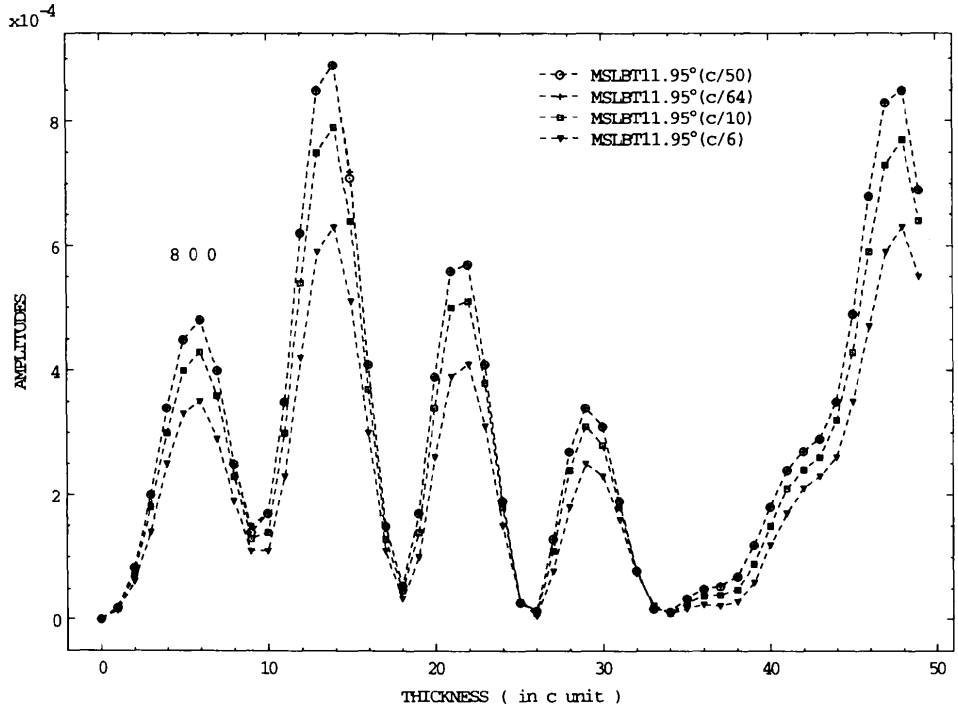

Fig. 9. Plots of the amplitudes of the 800 diffraction beam against crystal thickness, calculated by the MSBT with different slice thicknesses. Meanings of the symbols are the same as in Fig. 6.

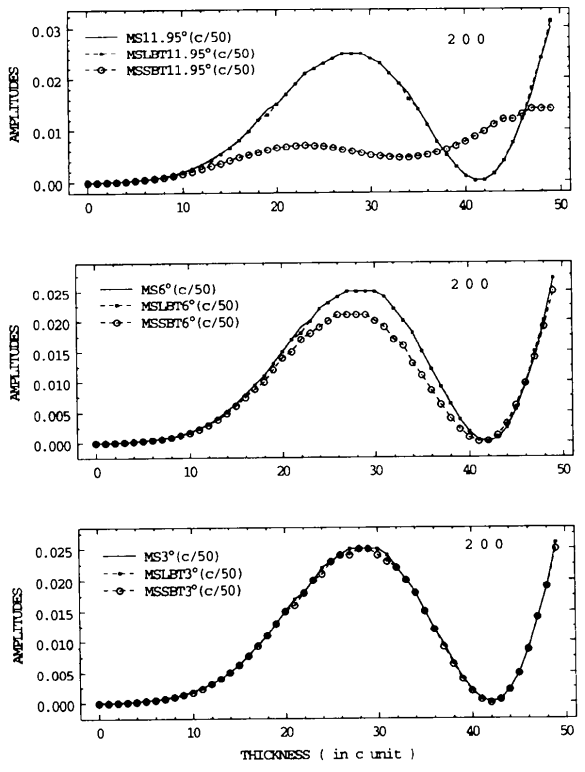

Fig. 10. Plots of the amplitudes of the 200 diffraction beam against crystal thickness, calculated by the two MSBT formulations, the MSLBT [equation (4)] and the MSSBT [equation (7)]. Meanings of the symbols are the same as in Fig. 6.

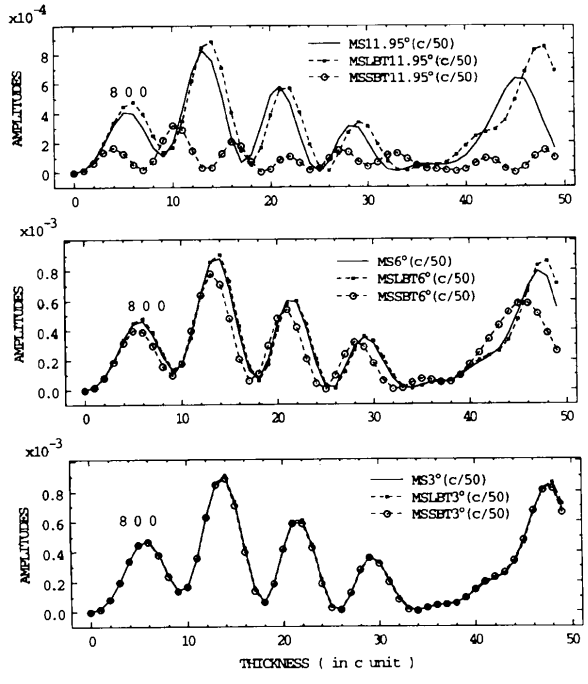

Fig. 11. The same as for Fig. 10 but for the 800 beam.

what are included are all those pointing towards the part $A'E'B'$ of the sphere, which covers the back-scattering wave vectors towards the part $B'B$ but excludes the forward-scattering wave vectors towards the part $A'A$. This could be the reason why the MSSBT is accurate for small tilt angles but invalid for large tilt angles. The small-angle scattering approximation used by Wang to obtain the same propagator as that in the MSSBT seems to enhance this explanation, since only if the small-angle scattering assumption holds and at the same time the tilt angle is not too large will the neglect of 'back scattering' $A'C'B'$ not cover a significant part of the correct forward-scattering AEB for the tilted beam.

However, it is hard to clearly explain what leads to the difference between the MSLBT and the MSSBT. We have seen that in order to obtain the MSLBT we write $\Psi(\mathbf{r}) = \varphi(\mathbf{r})\exp(2\pi i k_z z)$ and neglect $\partial^2\varphi/\partial z^2$, while we write $\Psi(\mathbf{r}) = \varphi(\mathbf{r})\exp(2\pi i k z)$ and neglect $\partial^2\varphi/\partial z^2$ to obtain the MSSBT. These two approximations are obviously different. With respect to Fig. 16(*b*), we can roughly say that $\partial^2\varphi/\partial z^2$ represents the complete 'back scattering' towards $A'C'B'$, which is determined by k, while $\partial^2\varphi/\partial z^2$ indicates those scattering towards $A''C''B''$, which is determined by k_z. So in fact the MSLBT does not completely lose all the 'back-scattering' effects towards $A'C'B'$, and

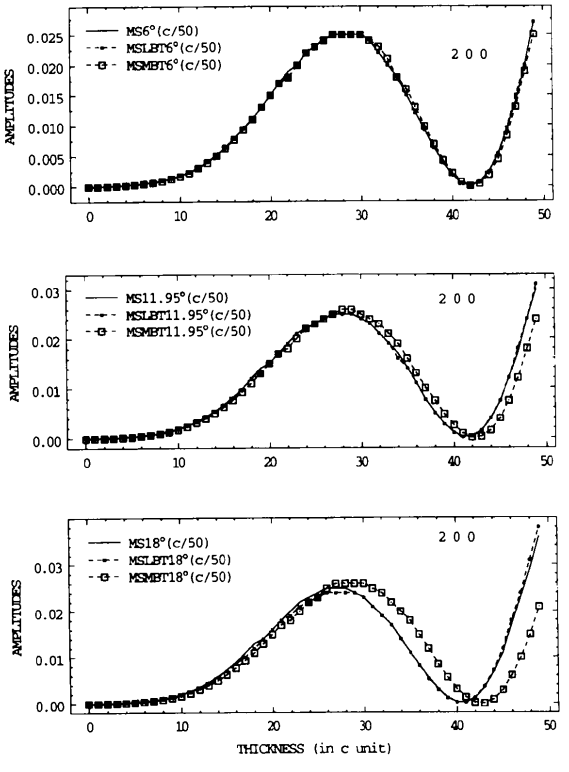

Fig. 12. The same as for Fig. 10 but for comparison between the MSLBT [equation (4)] and the MSMBT [equation (8)].

therefore is more accurate for large tilts (since in that case k_z is obviously less than k). For small tilts, however, k_z tends to k and these two formulations become the same. On other hand, from Wang's derivation, which leads to the same phase grating as that in the MSLBT, we see that the 'back scattering' in the MSLBT seems to be corrected so as to be closer to the correct back scattering for the tilted beam.

However, the 'back scattering' resulting in a MSBT formula will never be the correct one for a tilted beam as long as the slice is not taken perpendicular to the incident beam and the potentials are not projected along the beam direction. So, from this point of view, maybe Ishizuka's original MSBT formula would be more accurate than others. But this remains to be tested.

6.2. *HOLZ calculations for non-orthogonal crystals*

For calculating the HOLZ effects in triclinic and monoclinic (in case the incident beam is along the c axis of the monoclinic structure) crystals, the slices have to be chosen parallel to the ab plane of the crystals and the MSLBT should be used. However, if the θ angle between the c axis and the normal direction of the ab plane is too large, *e.g.* for the angle of 30°, the MSLBT can be inaccurate. To be reliable, we may conclude the following: (*a*) For the calculation of the large-angle resonant HOLZ effects, the MSLBT is accurate for the θ angles around 10° or less. (*b*) When only the lower-order HOLZ effects due to the top–bottom atomic layers of the crystals are involved (Stobbs, Boothroyd & Stobbs, 1989; Marks,

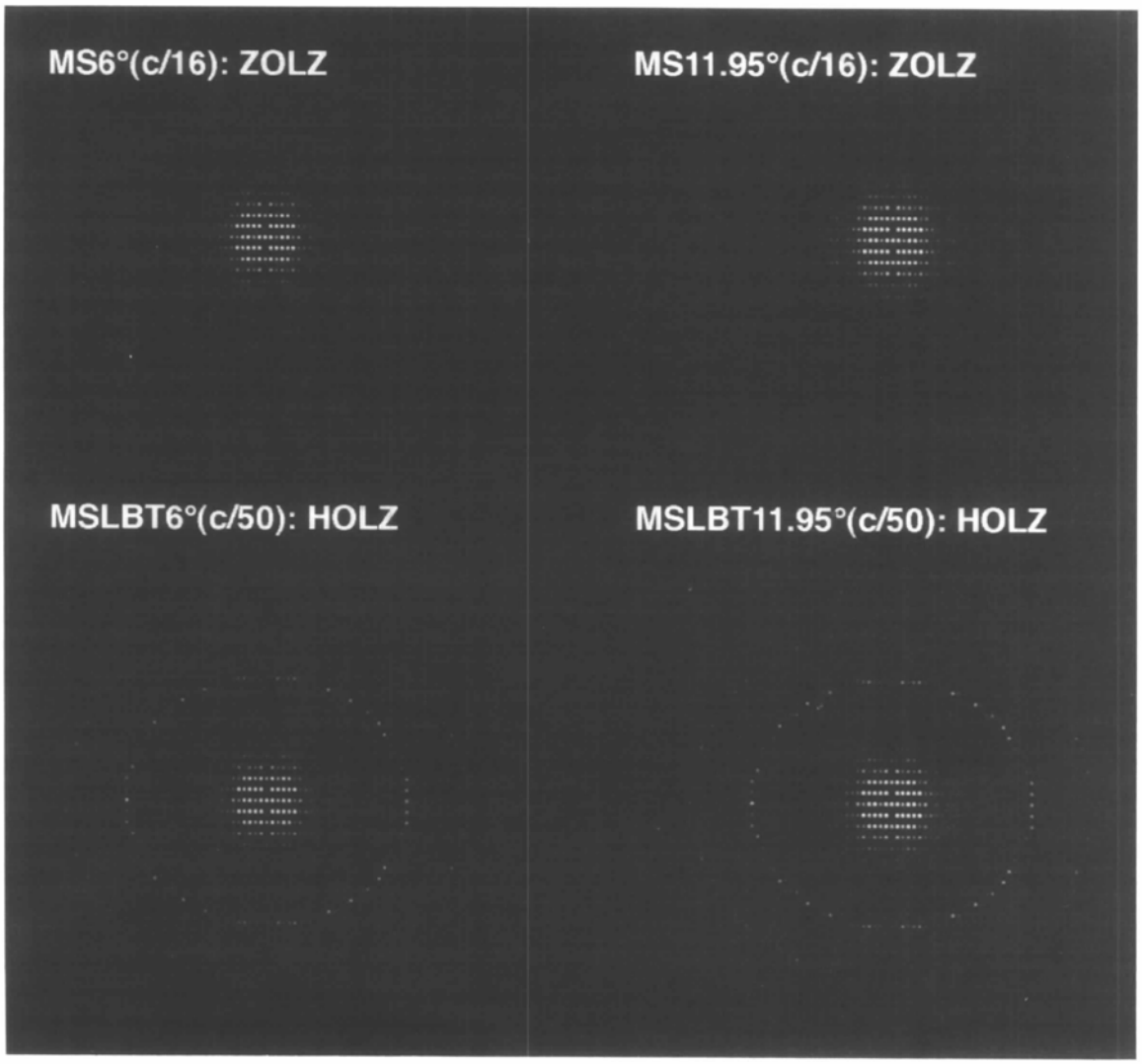

Fig. 13. Calculated diffraction patterns for $Na_2Ti_3O_7$ monoclinic structures, where the ZOLZ patterns are obtained by neglecting the potential variation along the c axis while the HOLZ patterns are obtained by including the potential variation. Meanings of the symbols are the same as in Fig. 6.

1992), *e.g.* when the c parameter is quite small and therefore the large-angle resonant HOLZ effects are not important, the MSLBT can be used until the θ angle is as large as 20°.

In the calculated HOLZ reflection patterns (Fig. 13), we can see that for monoclinic structures HOLZ reflections like 25,0,1 and $\bar{2}5$,0,1 are not centrosymmetric. This can easily be understood from the Ewald-sphere configuration (Fig. 2*b*). But the interesting thing shown in Figs. 13 and 14 is that ZOLZ reflections like $h00$ and $\bar{h}00$ are also not centrosymmetric and this cannot be expected from the Ewald-sphere configuration (the kinematic approximation) as well as the dynamical calculations in which the projection approximation (neglecting HOLZ effects) is used.

For orthogonal structures, it is believed that the large-angle resonant HOLZ effects normally do not yield obvious effects in HRTEM images and therefore can be neglected in image simulations (Qin & Urban, 1990; Chen *et al.*, 1996). This conclusion may not be valid for the cases of triclinic and monoclinic crystals. We know that, in the case of orthogonal structures, the large-angle resonant HOLZ effects with very weak intensities only slightly influence the intensities of ZOLZ patterns but not the symmetry. In other words, if Friedel's law holds under the projection approximation, it will still hold after including the large-angle resonant HOLZ effects. However, for triclinic and monoclinic crystals, Friedel's law will never hold if large-angle resonant HOLZ effects are involved. This non-symmetrical feature of ZOLZ patterns could yield observable effects in the HRTEM images that cannot be interpreted by image simulation with the projection approximation.

Finally, one important issue that should be addressed is that for HOLZ calculations the consistency between the multislice method (even without tilt) and the Bloch-wave method has thus far not been tested, although the equivalence between the two methods has been shown by the calculations for ZOLZ (*e.g.* Self *et al.*, 1983; Ma & Marks, 1990; Spence & Zuo, 1992). It is known that the so-called low-order HOLZ reflections (Self & O'Keefe, 1992), or the bulk-forbidden surface-allowed reflections (Marks, 1992), which appear at the forbidden positions of the ZOLZ plane when the number of unit cells in the beam direction is not an integer {*e.g.* Lynch (1971) for Au[111]} can easily be included in the MS calculation by using extra top–bottom slices (Chen *et al.*, 1996). But this type of HOLZ effect seems difficult for the Bloch-wave method to take into account. On the other hand, for the large-angle HOLZ reflections, the Bloch-wave method has been shown to be very successful [for reviews, see Spence & Zuo

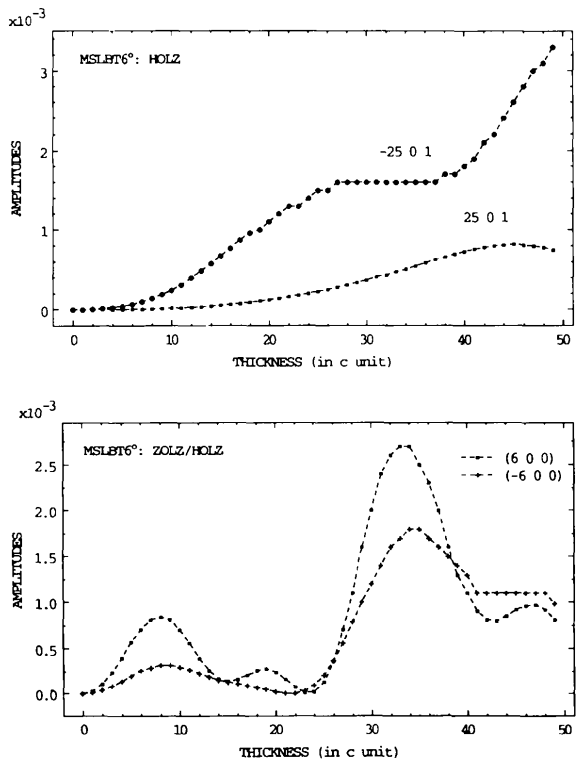

Fig. 14. Plots of the amplitudes of some HOLZ and ZOLZ reflections, showing the violation of Friedel's law in the diffraction of a monoclinic structure. Meanings of the symbols are the same as in Fig. 6.

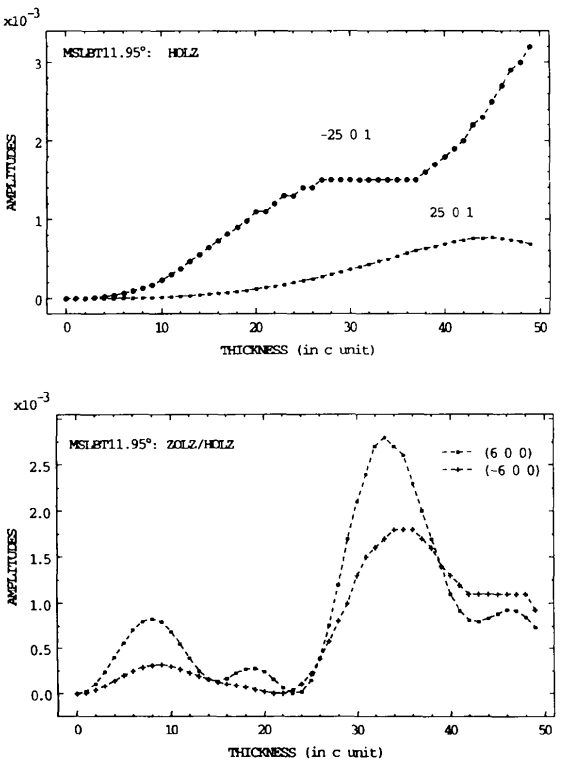

Fig. 15. The same as for Fig. 14 but for the structure with a different β angle.

(1992) for the reciprocal-space Bloch-wave method; Bird (1989) for the real-space Bloch-wave method]. But the MS has not been used much for calculating this type of HOLZ effect. The key question is how accurate the normal high-energy approximation is on which the MS is based. Although it has been pointed out that intuitively the parabola surface should be modified to the (Ewald) sphere surface, it is shown in our forthcoming work based on a rigorous approach that the sphere surface in fact is modulated by the crystal potential. So, for HOLZ effects, further theoretical work needs to be done.

7. Conclusions

Three existing MSBT formulations have been introduced in a unified form and the validity of these formulations has been evaluated with respect to the MS (without tilt). It is shown that the differences between these formulations can be summarized as follows: in MSSBT (the MS for small beam tilt), the slice thickness is measured along the normal direction of the slice plane, in MSLBT (large beam tilt), the slice thickness is measured along the incident-beam direction, and, in MSMBT (for medium beam tilts), the slice thickness for the propagator differs from that for the phase grating. The accuracy of each formulation is a function of the tilt angle. For small tilt angles less than 3°, these three formulations give exactly the same results. For tilt angles as large as 20°, only the MSLBT results are still very close to the MS results. The MSSBT is valid up to 6°, while the MSMBT is almost as accurate as the MSLBT up to 12°.

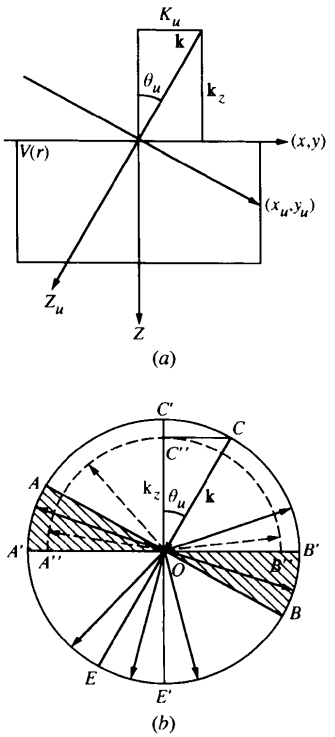

Fig. 16. Illustration of the back scattering in the case of inclined illumination: (*a*) in real space; (*b*) in reciprocal space with the Ewald sphere.

For calculating the HOLZ effects from triclinic and monoclinic (when the incident beam is along the *c* axis) crystals, the slices have to be taken parallel to the *ab* plane of the crystals and the MSLBT should be used. For the large-angle resonant HOLZ effects, the MSLBT can be used if the θ angle between the *c* axis and the normal direction of the *ab* lattice plane of the crystal is around 10° or less, while for the lower-order HOLZ effects the MSLBT may be used until the θ angle is as large as 20°.

For triclinic and monoclinic crystals, the large-angle resonant HOLZ effects dynamically influence not only the intensity but also the symmetry of ZOLZ diffraction patterns and this may yield observable effects in the HRTEM images. So, for simulating the HRTEM images of triclinic and monoclinic crystals, one may not simply use the projection approximation except when the *c* parameter is quite small so that the large-angle resonant HOLZ reflections do not occur.

APPENDIX *A*

Following Ishizuka's (1982) derivation, Wang (1995) obtained the following MSBT formula in its original form:

$$\Phi(\mathbf{b}, z)=[(K/K_z)P'(\mathbf{b},z-z_0)]*\{\exp[i\sigma(K/K_z)V(\mathbf{b})]\Phi(\mathbf{b},\mathbf{z_0})\} \tag{18}$$

with the potential $V(\mathbf{b})$ projected along the normal direction of the slice plane and the propagator

$$P'(\mathbf{b}, \Delta, z = z - z_0) = (1/i\lambda\Delta z)\exp[2\pi i(K - K_z)\Delta z] \times \exp[(\pi i b^2/\lambda\Delta z) - 2\pi i\mathbf{K}_b \cdot \mathbf{b}]. \tag{19}$$

In our notation, (18) and (19) should be rewritten as

$$\Phi_n^{\mathbf{K}_u}(\mathbf{R}, n\varepsilon) =[(k/k_z)P'(\mathbf{R}, \varepsilon)] * \{\exp[i\sigma(k/k_z)\varepsilon V_n^p(\mathbf{R})] \times \Phi_{n-1}^{\mathbf{K}_u}[\mathbf{R}, (n-1)\varepsilon]\} \tag{20}$$

with

$$P'(\mathbf{R}, \varepsilon) = (1/i\lambda\varepsilon)\exp[2\pi i(k - k_z)\varepsilon]\exp[(\pi i\mathbf{R}^2/\lambda\varepsilon) - 2\pi i\mathbf{K}_u \cdot \mathbf{R}], \tag{21}$$

where $*$ indicates a convolution product.

Taking a 2D Fourier transformation over (21), we obtain

$$\int P'(\mathbf{R},\varepsilon)\exp(-2\pi i\mathbf{K}\cdot\mathbf{R})\,d\mathbf{R}$$
$$= \exp[2\pi i(k-k_z)\varepsilon]\exp[-\pi i\lambda\varepsilon(2\mathbf{K}_u\cdot\mathbf{K}+\mathbf{K}_u^2)]$$
$$\times (1/i\lambda\varepsilon)\int \exp[(\pi i/\lambda\varepsilon)(\mathbf{R}-\lambda\varepsilon\mathbf{K}_u)^2]$$
$$\times \exp[2\pi i\mathbf{K}\cdot(\mathbf{R}-\lambda\varepsilon\mathbf{K}_u)]\,d(\mathbf{R}-\lambda\varepsilon\mathbf{K}_u)$$
$$= \exp[2\pi i(k-k_z)\varepsilon]\exp[-\pi i\lambda\varepsilon(\mathbf{K}+\mathbf{K}_u)^2]. \quad (22)$$

So the convolution of the propagator by a wave function will be

$$(k_z/k)P'(\mathbf{R},\varepsilon) * \Phi(\mathbf{R}) = (k_z/k)\exp[2\pi i(k-k_z)\varepsilon]$$
$$\times \int\{\exp[-\pi i\lambda\varepsilon(\mathbf{K}+\mathbf{K}_u)^2]\varphi(\mathbf{K})\}$$
$$\times \exp(2\pi i\mathbf{K}\cdot\mathbf{R})\,d\mathbf{K}. \quad (23)$$

On the other hand, we have

$$\exp\{\varepsilon[(i\lambda\Delta/4\pi) - \lambda\mathbf{K}_u\cdot\nabla - \pi i\lambda\mathbf{K}_u^2]\}\Phi(\mathbf{R})$$
$$= \exp[(i\lambda\varepsilon/4\pi)(\nabla + 2\pi i\mathbf{K}_u)^2]\Phi(\mathbf{R})$$
$$= \left\{\sum_m (1/m!)[(i\lambda\varepsilon/4\pi)(\nabla+2\pi i\mathbf{K}_u)^2]^m\right\}$$
$$\times \int \varphi(\mathbf{K})\exp(2\pi i\mathbf{K}\cdot\mathbf{R})\,d\mathbf{K}$$
$$= \int\left\{\sum_m (1/m!)[(i\lambda\varepsilon/4\pi)(2\pi i)^2(\mathbf{K}+\mathbf{K}_u)^2]^m\right\}$$
$$\times \varphi(\mathbf{K})\exp(2\pi i\mathbf{K}\cdot\mathbf{R})\,d\mathbf{K}$$
$$= \int\{\exp[-\pi i\lambda\varepsilon(\mathbf{K}+\mathbf{K}_u)^2]\varphi(\mathbf{K})\}\exp(2\pi i\mathbf{K}\cdot\mathbf{R})\,d\mathbf{K}. \quad (24)$$

Comparing (23) with (24), we therefore have

$$\underline{(k_z/k)P'(\mathbf{R},\varepsilon)*}\Phi(\mathbf{R}) = \underline{(k_z/k)\exp[2\pi i(k-k_z)\varepsilon]}$$
$$\underline{\times \exp\varepsilon[(i\lambda\Delta/4\pi)}$$
$$\underline{-\lambda\mathbf{K}_u\cdot\nabla - \pi i\lambda\mathbf{K}_u^2]}\Phi(\mathbf{R}). \quad (25)$$

Dropping the constant factor (for single-beam illumination), $(k_z/k)\exp[2\pi i(k-k_z)\varepsilon]$, the MSBT formula, (20), can therefore be rewritten as

$$\Phi_n^{\mathbf{K}_u}(\mathbf{R}) = \exp\{\varepsilon[(i\lambda\Delta/4\pi) - \lambda\mathbf{K}_u\cdot\nabla - \pi i\lambda\mathbf{K}_u^2]\}$$
$$\times \exp[i\sigma\varepsilon_u V_n^p(\mathbf{R})]\Phi_{n-1}^{\mathbf{K}_u}(\mathbf{R}). \quad (26)$$

We can see that in (26) the 'slice thickness' in the phase grating is measured along the incident-beam direction, $\varepsilon_u = (k/k_z)\varepsilon$, while the slice thickness in the propagator is measured along the normal direction of the slice plane.

This text presents research results partly sponsored by the Belgian program on InterUniversity Poles of Attraction initiated by the Belgian State, Prime Minister's Office of Science Policy Programming. The scientific responsibility is assumed by the authors. The authors are grateful to Professors J. Van Landuyt and G. Van Tendeloo for their enduring support and careful reading of the manuscript.

References

Andersson, S. & Wadsley, A. D. (1961). *Acta Cryst.* **14**, 1245–1249.
Bird, D. M. (1989). *J. Electron Microsc. Tech.* **13**, 77–97.
Chen, J. H., Op de Beeck, M. & Van Dyck, D. (1996). *Microsc. Microanal. Microstruct.* **7**, 27–47.
Chen, J. H., Van Dyck, D., Op de Beeck, M., Broeckx, J. & Van Landuyt, J. (1995). *Phys. Status Solidi A*, **150**, 13–22.
Chen, J. H., Wang, Y. M., Luo, X. J., Ding, L. Y. & Cheng, X. L. (1995). *Philos. Mag. Lett.* **71**, 33–37.
Cowley, J. M. (1981). *Diffraction Physics*, ch 11, p. 240. Amsterdam/New York/Oxford: North-Holland.
Cowley, J. M. & Moodie, A. F. (1957). *Acta Cryst.* **10**, 609–619.
Goodman, P. & Moodie, A. F. (1974). *Acta Cryst.* A**30**, 280–290.
Ishizuka, K. (1982). *Acta Cryst.* A**38**, 773–779.
Ishizuka, K. & Uyeda, N. (1977). *Acta Cryst.* A**33**, 740–749.
Lynch, D. F. (1971). *Acta Cryst.* A**27**, 399–407.
Ma, Y. & Marks, L. D. (1990). *Acta Cryst.* A**46**, 11–32.
Marks, L. D. (1992). *Ultramicroscopy*, **38**, 325–332.
Qin, L. C. & Urban, K. (1990). *Ultramicroscopy*, **33**, 159–166.
Self, P. G. & O'Keefe, M. A. (1992). *High-Resolution Transmission Electron Microscopy and Associated Techniques*, p. 259. Oxford University Press.
Self, P. G., O'Keefe, M. A., Buseck, P. R. & Spargo, A. E. C. (1983). *Ultramicroscopy*, **11**, 35–52.
Spence, J. C. H. & Zuo, J. M. (1992). *Electron Microdiffraction*, p. 309. New York/London: Plenum Press.
Stobbs, S. H., Boothroyd, C. B. & Stobbs, W. M. (1989). *Inst. Phys. Conf. Ser.* No. 98, p. 387.
Van Dyck, D. (1979). *Phys. Status Solidi A*, **52**, 283–292.
Van Dyck, D. (1980). *J. Microsc.* **119**, 141–152.
Van Dyck, D. & Coene, W. (1984). *Ultramicroscopy*, **15**, 29–40.
Wang, Z. L. (1995). *Elastic and Inelastic Scattering in Electron Diffraction and Imaging*. New York/London: Plenum Press.